Studies of Relativistic Backward Wave Oscillators: Comparison between Theory and Experiment

B. Levush, T. Antonsen Jr., A. Bromborsky[a]
W. R. Lou, D. Abe, S. Miller, Y. Carmel, J. Rodgers,
V. Granatstein, and W. Destler

Laboratory for Plasma Research, University of Maryland
College Park, MD 20742-3511

ABSTRACT

Microwave sources based on backward-wave oscillators driven by relativistic electron beams are capable of producing high power coherent radiation in the cm and mm wavelength regime. Although there have been a number of experiments reported over the last decade on this topic, there are only a few publications providing a theoretical description of these devices. Thus, there is a need for theoretical models which can be compared in detail with the experimental data. This work is devoted to filling this need and applied to the University of Maryland backward wave oscillator experiment. It is shown that the theoretical predictions for the threshold current to start the oscillations, the frequency characteristics, and the efficiency of the device compared favorably with the experimental data.

1. INTRODUCTION

One of the most successful examples of high power microwave sources utilizing high current relativistic electron beam is the Backward-Wave Oscillator (BWO).[1,2] The device consists of a periodic metallic structure into which a high current relativistic electron beam is injected, see Fig. 1. The beam is usually confined by a strong axial magnetic field. The slow wave structure reduces the phase velocity of electromagnetic (EM) waves below the vacuum speed of light so that the electrons in the relativistic electron beam can give up energy directly to one of the eigenmodes of the structure. The theoretical model which we used to simulate the operation of the BWO is based on the model published in Ref. 3, which is essentially the same as has been studied in connection with traveling wave devices for decades.[4] We extended this model by taking into account the effect of reflections of the electromagnetic wave at both boundaries of the interaction region.[5] The model can be described as follows. An electron beam which is injected into a slow wave structure interacts weakly with an electromagnetic wave of the vacuum structure. The interaction is weak in the sense that, if examined over a region of space of the size of the order of one period of the structure, the electromagnetic field has the temporal and spatial dependences of a wave in the empty structure. The effect of the beam is to cause the electromagnetic wave to vary slowly in time and axial distance.

The beam electrons are assumed to be guided by an infinitely strong axial magnetic field. Thus only motion in the axial dimension is considered. The model assumes that the backward propagating wave after interacting with the beam suffers reflection at the beam entrance of the cavity (where it is cut off by a drift tube) and becomes a forward wave. The forward wave does not interact with the beam, but it may be reflected at the beam exit of the cavity. The reflected forward wave becomes a backward wave which can interfere constructively or destructively with amplified backward wave. In a realistic structure, the total round trip amplitude reflection coefficient can be in excess of 0.7 and, thus, can be expected to greatly influence the operation of the device.

We used this theory to simulate the operation of University of Maryland BWO.[6]

2. BASIC FORMULATION

In this section we will review the basic model of the backward-wave oscillator interaction that was developed in Ref. 5. We begin with the expression for the high frequency electromagnetic field for one transverse mode:

$$\mathbf{E}(\mathbf{x},t) = \left\{\epsilon_- e^{ik_- z-\omega t)}\mathbf{E}_p(\mathbf{x},k_-) + \epsilon_+ e^{i(k_+ z-\omega t)}\mathbf{E}_p(\mathbf{x},k_+)\right\} + c.c., \quad (1)$$

0-8194-0775-5/92/$4.00

$$\mathbf{B}(\mathbf{x},t) = \left\{\epsilon_- e^{i(k_- z-\omega t)}\mathbf{B}_p(\mathbf{x},k_-) + \epsilon_+ e^{i(k_+ z-\omega t)}\mathbf{B}_p(\mathbf{x},k_+)\right\} + c.c., \tag{2}$$

where $\epsilon_\pm(z,t)$ is the slowly varying amplitude of the electromagnetic wave, $\mathbf{E}_p(\mathbf{x},k_\pm)$ and $\mathbf{B}_p(\mathbf{x},k_\pm)$ are the complex amplitudes for the electromagnetic fields which represent the solutions for waves in the empty structure for the forward, "+", and backward wave "-", respectively. The fields $\mathbf{E}_p(\mathbf{x},k_\pm)$ and $\mathbf{B}_p(\mathbf{x},k_\pm)$ satisfy Maxwell's equations for waves with frequency ω and Floquet wave number $k_\pm$. The wave numbers k_- and k_+ satisfy $\omega = \omega(k_-) = \omega(k_+)$ and for symmetric structures are related by $k_- + k_+ = 2\pi/d$, (d is the period of the structure) see Fig. 2.

The slowly varying amplitude for the backward wave ϵ_- satisfies the following envelope equation

$$\frac{\partial\epsilon_-}{\partial t} + v_{g,-}\frac{\partial\epsilon_-}{\partial z} = -\oint dz \int d^2\mathbf{x}_\perp \mathbf{E}_p^*(\mathbf{x},k_-)\cdot\mathbf{j}\exp[-i(k_- z-\omega t)]/U, \tag{3}$$

where

$$U = \int dz \int d^2\mathbf{x}_\perp \frac{|\mathbf{E}_p|^2 + |\mathbf{B}_p|^2}{4\pi} \tag{4}$$

is the electromagnetic energy per $|\epsilon|^2$ contained in one period and

$$v_{g,-} = \int dz \int d^2\mathbf{x}_\perp \frac{c}{4\pi}\hat{z}\cdot(\mathbf{E}_p(\mathbf{x},k_-)\times\mathbf{B}_p^*(\mathbf{x},k_-) + \mathbf{E}_p^*(\mathbf{x},k_-)\times\mathbf{B}_p(\mathbf{x},k_-))/U \tag{5}$$

is the group velocity for the vacuum backward electromagnetic wave. The electron beam interacts only with the backward wave, thus the evolution equation for the amplitude ϵ_+ has no source term

$$\frac{\partial\epsilon_+}{\partial t} + v_{g,+}\frac{\partial\epsilon_+}{\partial z} = 0. \tag{6}$$

However, the forward wave is coupled with the backward wave at the boundaries of the cavity. Thus, Eqs. (3) and (6) are augmented by boundary conditions at $z = 0$,

$$\epsilon_+(z=0) = \rho_0 e^{i\phi_0}\epsilon_-(z=0), \tag{7}$$

and at $z = L$,

$$\epsilon_+(z=L)e^{ik_+L}\rho_L e^{i\phi_L} = \epsilon_-(z=L)e^{ik_-L}, \tag{8}$$

where ρ_0, ϕ_0, ρ_L and ϕ_L determine the complex reflection coefficients at the left and right boundaries, respectively.

The high frequency current density, $\mathbf{j}$, appearing in (3) is constructed from individual particle trajectories. The beam electrons are assumed to be guided by an infinitely strong axial magnetic field. Thus, only motion in the axial dimension is considered. A beam particle is characterized by its phase $\psi = kz - \omega t$, and its energy γmc^2 where m is the electron mass, $\gamma = (1 - v^2/c^2)^{-1/2}$ is the relativistic factor and v is the particle's velocity. As a particle travels down the interaction region its phase evolves according to

$$\frac{\partial\psi}{\partial t} + v_z\frac{\partial\psi}{\partial z} = \frac{d\psi}{dt} = kv_z - \omega, \tag{9}$$

and the rate of change of particle energy can be written

$$\frac{d\gamma}{dt} = \frac{qv_z}{mc^2}(\epsilon_-\bar{E}_{zp})e^{i\psi} + c.c., \tag{10}$$

where the axial field $\bar{E}_{zp}$ is evaluated at the transverse location of the beam electron and the overbar on $\bar{E}_{zp}$ indicates spatial average over one period of the structure.

The action of the high frequency fields is to cause the beam particles to become bunched in phase, ψ. This causes the axial beam current to become temporally and spatially modulated. If the beam current is represented in terms of an ensemble of particles with axial position z, therefore the right-hand side of Eq. (3) can be replaced by the following average,[5]

$$Id\bar{E}^*_{zp}(r_b)\langle e^{-i\psi}\rangle, \tag{11}$$

where I is the total beam current and the average is taken over an ensemble of particles entering the device with continuous distribution of phases between 0 and 2π.

This completes the description of our governing equations for backward wave oscillator. In Ref. 5 the dynamics of BWO's was investigated using this equation. However, certain modifications are required for a more realistic description of the device operation.

2.1. The A.C. space charge effect

The beam bunching induces a space charge axial electric field which is proportional to the beam density. This electric field is added to the electromagnetic electric field in the equation of motion (10)

$$\frac{d\gamma}{dt} = \frac{qv_z}{mc^2}(\epsilon_- \bar{E}_{zp} + \bar{E}^{(1)}_{zp})e^{i\psi} + c.c., \tag{12}$$

where $\bar{E}^{(1)}_{zp}$ is the small first order space charge field spatial averaged over one period of the structure. This field was evaluated for the case of an infinite, homogeneous beam and has the following form[5]

$$\bar{E}^{(1)}_{zp} = \frac{-i4\pi I k_\perp^2}{\omega} C_2 \langle e^{-i\psi}\rangle.$$

For the case of an annular beam in a smooth wall waveguide the coefficient C_2 can be calculated analytically[5] and is given by

$$C_2 = \frac{1}{2\pi} I_0(k_\perp r_b) K_0(k_\perp r_b) \left[1 - \frac{K_0(k_\perp r_w) I_0(k_\perp r_b)}{K_0(k_\perp r_b) I_0(k_\perp r_w)}\right], \tag{13}$$

where I_0 and K_0 are modified Bessel functions and r_w is the radius of the conducting wall. For periodic structure calculations we use $r_w = r_{av}$, where r_{av} is the average wall radius of the periodic structure.

2.2. Modeling the finite pulse length

In a typical experiment with an intense relativistic beam, the voltage and current have a duration of a couple hundred nanoseconds with a rise time of the order of several tens of nanoseconds. To simulate this situation we allow the beam parameters in our model to become functions of the time. We take a rising exponential as a model for the beam voltage:

$$V(t) = V_p(1 - e^{-(t+t_p)/t_r}). \tag{14}$$

We also assume that the current waveform is described by the following expression:

$$I(t) = I_p(1 - e^{-(t+t_p)/t_r})^\rho, \tag{15}$$

where t_r is the rise time and t_p, I_p and V_p are parameters chosen to best model the measured characteristics of the beam. Further, we assume that the Child-Langmuir law is approximately valid, hence $\rho = 1.5$. To model the termination of the beam pulse we assume that at some point in time, $t = t_f$, the current and voltage start to drop exponentially. The values of the current and voltage at $t = t_f$ are denoted as I_{max} and V_{max}, respectively.

2.3. Modeling voltage depression

The next modification of the model is related to the electron beam D.C. space charge effect. It is well known that the electron beam slows down as it enters the RF structure due to buildup of an electrostatic potential (voltage depression) inside the metallic structure.[7] This voltage depression will reduce the electron beam energy $mc^2\gamma_0$ (where $\gamma_0 = 1 + V/mc^2$) by some amount $mc^2\Delta\gamma$. To evaluate $\Delta\gamma$ we used the following formula:[7]

$$\Delta\gamma = 2\frac{I(t)}{I_A}\ell n\left(\frac{r_{av}}{r_b}\right)\left(1 - \frac{1}{(\gamma_0 - \Delta\gamma)^2}\right)^{-1/2} \tag{16}$$

Previously, we only specified the value of the initial relativistic factor inside the structure, γ_i. However, now the beam current and voltage leaving the diode are time-dependent and are evaluated according to the model given by Eqs. (14)–(15), $\gamma_0 = 1 + V(t)/mc^2$. Thus, the initial value for the relativistic factor γ_i is evaluated as follows: $\gamma_i = \gamma_0 - \Delta\gamma$.

The above equations are solved numerically. The results of these simulations are compared with the experimental data from the University of Maryland BWO experiment.[6]

3. STARTING CURRENT: CALCULATIONS AND MEASUREMENTS

The starting current is the minimum beam current required to start oscillations from noise in the RF structure. The starting current for a finite length sinusoidal slow wave structure has been calculated by a number of authors.[3,8]

The expression for the starting current for a cold beam in our notation takes the form

$$I_{st} = \frac{I_A}{4\pi}\left(\frac{d}{L}\right)^3 \frac{\gamma_i^3\beta_{zi}^2}{(k_*d)}\frac{\beta_g(\omega_*)}{C(r_b,\omega_*)}\tilde{I}_{st}, \tag{17}$$

where $I_A = mc^3/q = 1.7 \times 10^4$ Amps and $\beta_{zi} = (1 - 1/\gamma_i^2)^{-1/2}$ is the initial normalized axial velocity of the injected beam. The resonant frequency, ω_*, appearing in Eq. (17), is defined as the intersection of the dispersion curve $\omega(k)$ of the cold slow wave structure and the electron beam Doppler line $\omega = kv_{zi}$, where $v_{zi} = c\beta_{zi}$, see Fig. (2). This also determines the resonance wave number $k_* = \omega_*/v_{zi}$ and the group velocity $\beta_g(\omega_*)$. The coupling coefficient $C(r)$ is defined as

$$C(r) = \frac{|\int_0^d \frac{dz}{d} E_{zp}(z,r)|^2}{\int_0^d \frac{dz}{d}\int_0^{r_w(z)} \frac{2\pi r dr}{d^2}\{|\mathbf{E}_p(r,z)|^2 + |\mathbf{B}_p(r,z)|^2\}}, \tag{18}$$

where $r_w(z)$ is the wall radius of the periodic structure.

The coupling coefficient $C(r = r_b)$ is the measure of strength of the axial electric field component which couples with the beam.

The quantity $\tilde{I}_{st}$ is a dimensionless number which we refer to as the "universal" starting current. Thus, the dependence of the actual starting current on physical parameters of the device enters through the factors multiplying $\tilde{I}_{st}$. Without end reflections the "universal" starting current takes on a value $\tilde{I}_{st} = 7.7$.

When reflections of the EM wave are included, Eq. (17) remains valid; however, the "universal" starting current now depends on the magnitude of the combined reflection coefficient, $R = \rho_0\rho_L$, and the total round trip phase change, $2k_*L + \phi_r$, at frequency ω_* for the EM wave, where $\phi_r = \pi - \phi_0 - \phi_L$. We have determined this dependence via numerical solution of the nonlinear equations in the linear regime.

We used the results of these calculations to obtain the starting current versus electron gun voltage in the RF structure used in our experiment.

The structure used in the experiment was a circularly symmetric waveguide of 8 period long with average radius, r_{av}=1.5 cm, sinusoidal ripples of period d = 1.67 cm, height $\Delta = (r_{max} - r_{min})$= .82 cm. The dispersion curves, coupling coefficients, and reflection coefficients were calculated using a separate code.[9]

In Fig. 3 a plot of start current versus diode voltage for the structure is shown. We observe that the maximum starting current is about 50 Amps and the minimum is about 5 Amps. We also see that a 30% variation in voltage may lead to a factor of two or three variations in starting current. This starting current is much smaller than the current which is typically used in the device.

A series of low current experiments attempting to measure the start current have been conducted.[6] The main challenge in the experiment was to achieve BWO operation over a wide range of electron beam energy and current. Since for a particular gun geometry the variation in the beam current is limited, we built a number of electron guns which allowed us to cover a broad range of beam parameters. The Volt-Ampere characteristics of one such gun is shown in Fig. 5. The black square marked on the curve indicates the parameters of the BWO (I_{max}=77 Amp and V_{max}=289 kV) for which the theoretical predictions are compared with the experimental data. This is the current below which no radiation has been detected with the available detectors.

We find that the "measured starting current" is significantly above the calculated starting current. However, the comparison strictly speaking is not valid since the starting current is defined under the assumption that the flat top of the electron beam pulse is infinitely long.

In a typical BWO experiment the voltage and the current pulse have a finite duration with a finite rise time. For example, Fig. 4 shows the oscilloscope traces of the electron beam current and voltage for the case labeled by the black square on the Volt-Ampere line in Fig. 3. Figure 4 also shows the corresponding oscilloscope trace of the radiated power. The simulations were performed with the experimentally measured waveforms for voltage and current, and the results for the radiation output power in normalized units versus time are shown in Fig. 5. When a slightly lower current (65 Amps) is used in the simulation, the maximum power is reduced by a factor of sixty. This shows that the time-dependent start current calculation is in a better agreement with the experiment.

4. BWO OPERATION: SIMULATIONS AND MEASUREMENTS

In this section the experimental and theoretical investigations of the dynamics of the BWO in a wide range of beam voltage (from 250 kV to 600 kV) and moderate values of the beam current (below 200 Amps) are presented. In all simulations we used the same parameters for the RF structure as we used for the starting current calculations. The electron beam radius is r_b = 0.775 cm. The duration of the electron beam pulse is 135 nsec. The beam current and the voltage reach the maximum value at time t_f = 105 nsec. We also assume in all simulations that at the start of the simulation the beam current reached 20% of the I_p value. All other parameters are collected in Table 1.

5. FREQUENCY MEASUREMENTS

For all values of the beam voltage and current given in Table 1 the measured frequency of the radiation turned out to be about the same, 8.5 GHz. In Fig. 6 the measured frequency (symbol (+)) versus voltage is shown.

The frequency of the device operation is commonly determined by the intersection of the dispersion curve of the slow wave structure and the electron beam Doppler line $\omega = kv_{zi}$ [Fig. 2]. Following such a procedure, we calculated the frequency of device operation using the values of the beam voltage and current from Table 1. The beam axial velocity is calculated using the depressed value for the beam voltage [Eq. (16)]. The obtained frequencies, f_*, are marked by the symbol (*) in Fig. 6. As expected, the calculated frequency is higher then observed, since the frequency pulling effect[5] is not included in this simple calculation.

To evaluate the frequency pulling effect on the frequency of the device operation, we resorted to numerical simulation. We used our time-dependent, self-consistent model with the finite "end" reflections to calculate the frequency pulling, Δf. The actual frequency of the BWO in GHz is obtained from the following formula

$$f = f_* - |\beta_{g-}|(30/L)(k_*L)(k/k_* - 1) + \Delta f$$

in which we choose the parameter k/k_* = 1.2. The values of f calculated using the parameters from Table 1 are denoted by the symbol (•) in Fig. 6. We find that the agreement between the measured and calculated frequencies is good.

5.1 Efficiency measurements and calculations

The peak efficiency of the device is defined as the ratio of the maximum output power to the beam power. We used three methods to measure the output power: the peak-up horn, the coupling whole connected to a short dispersive line with a detector at the end, and the same coupling whole connected to a long dispersive line with a detector at the end.[6] In general, the uncertainty in the measured power is ± 1.5 dB.

In Fig. 7 the experimental data is shown together with the calculated efficiency. The parameters of the beam and the parameters which have been used in the simulations are given in Table 1. The output power in the simulations has strong modulation in time, since the device is operating in the overbunch unstable region (the ratio of the operating current to the start current is large).[5] The measured output power does not exhibit such strong modulation. However, in the experiment the measured radiation power is affected by the response time of the detectors as well as the effects of dispersion between the device and detector. Therefore, to make adequate comparison, the averaging effect of the detector and the dispersion line is taken into account in the analyses of the calculated output power as it emerges from the interaction region. We used 1.5 nsec response time to simulate the averaging effect. The peak efficiency from these simulations are plotted in Fig. 7.

We find that the overall agreement of the measured and calculated efficiencies is quite good. Note that we did not perform simulations beyond 520 kV. This is because at this voltage the operating frequency is close to the cut-off frequency "π" mode and therefore the Eqs. (3) and (6) are not valid. Theoretical modeling of BWO operation close to the "π" mode operation will be given elsewhere.

6. SUMMARY

We have adopted the approach which has been developed for the description of microwave devices with inertial bunching to the case of relativistic BWO's with internal reflections.[5]

Taking into account the finite rise time and finite duration of the electron beam pulse, voltage depression and A.C. space charge effects, and the averaging effect of the finite response time of the experimental detection system we simulated the University of Maryland BWO experiment.[6] The simulation results are in a reasonable agreement with experimental data.

At this point we would like to make several comments about future work on the theoretical modeling of the device operation. First, the effect of a finite axial magnetic field on the oscillator operation is neglected in the present theoretical formulation. However, there are a number of experimental evidence that the output power in BWO's depends on the value of the axial magnetic field.[10] Next, there is experimental evidence that the electron beam may interact strongly with a number of transverse modes simultaneously.[11]

7. ACKNOWLEDGEMENTS

This work has been partially supported by the U.S. Army Harry Diamond Laboratories and Air Force Office of Scientific Research.

8. REFERENCES

(a) Harry Diamond Laboratories

1. N. F. Kovalev, M. I. Petelin, M. D. Raizer, A. V. Smorgonski, and L. E. Tsopp, JETP Lett., 138 (1973).
2. Y. Carmel, J. Ivers, R. E. Kribel, and J. Nation, Phys. Rev. Lett. **33**, 1278 (1974).
3. N. S. Ginzburg, S. P. Kuznetzov, and T. N. Fedoseeva, Sov. Radiophys. and Electron. **21**, 728 (1979).
4. J. R. Pierce, *Traveling-wave Turbes* (D. Van Nostrand Comp., Inc., Toronto, 1950).

5. B. Levush, T. Antonsen, Jr., A. Bromborsky, W. Lou, and Y. Carmel, IEEE Trans. of Plasma Sc., to be published (1992).

6. W. Lou, Ph.D. Thesis, University of Maryland, 1991.

7. R. B. Miller, *An introduction to the physics of intense charged particle beams* (Plenum Press, 1982).

8. J. A. Swegle, Phys. Fluids **30**, 1201 (1987).

9. A. Bromborsky, this issue.

10. Y. Carmel, W. R. Lou, T. M. Antonsen Jr., J. Rodgers, B. Levush, W. W. Destler, and V. L. Granatstein, Phys. Fluids B, to be published (1992).

11. J. M. Butler, C. B. Wharton, and S. Furukawa, IEEE Trans. Plasma Sci. **18**, 490 (1990).

TABLE 1. SIMULATION PARAMETERS

Parameters	1	2	3	4	5	6
I_{max}(kA)	0.095	0.102	0.105	0.104	0.147	0.150
$V_{\max}$(kV)	305	365	394	443	482	521
β_g	0.167	0.1423	0.132	0.116	0.105	0.095
k_*L	30.83	29.77	29.36	28.77	28.40	28.06
C_p	0.033	0.039	0.041	0.045	0.047	0.05
C_2	0.53	0.55	0.55	0.6	0.44	0.45
$\chi = I_{\max}/I_{\text{start}}$	8	6	9.5	21	29	30
R	0.78	0.83	0.84	0.86	0.87	0.89
ϕ_r(rad)	2.68	2.77	2.81	2.86	2.89	2.91

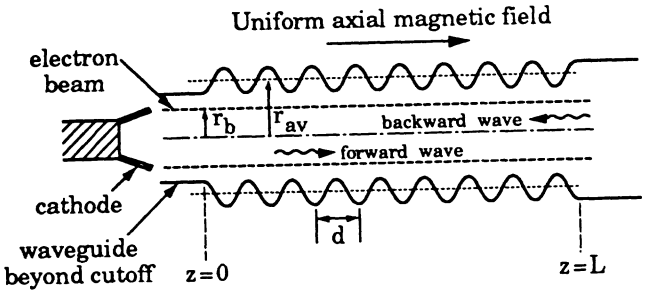

Fig. 1. A schematic picture of a BWO device. A thin annular relativistic electron beam of radius r_b is generated by a cathode with explosive emission and propagates along strong axial magnetic field inside of a cavity with ripple walls.

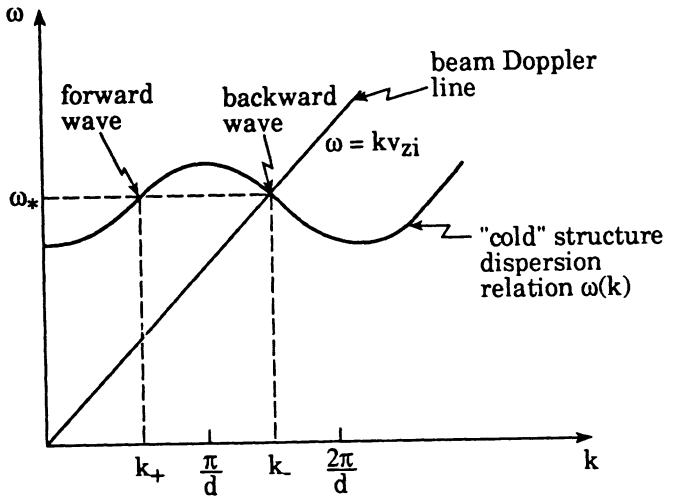

Fig. 2. A schematic picture of a dispersion relation, $\omega(k)$, of TM_{01} mode in an infinitely long periodic structure. The straight line which intersects the cold structure dispersion curve is the electron beam Doppler line, $\omega = kv_{zi}$, where v_{zi} is the beam initial velocity. The wave number k_- denotes the backward wave and k_+ denotes the forward wave, while the frequency for both waves in the same, ω_*.

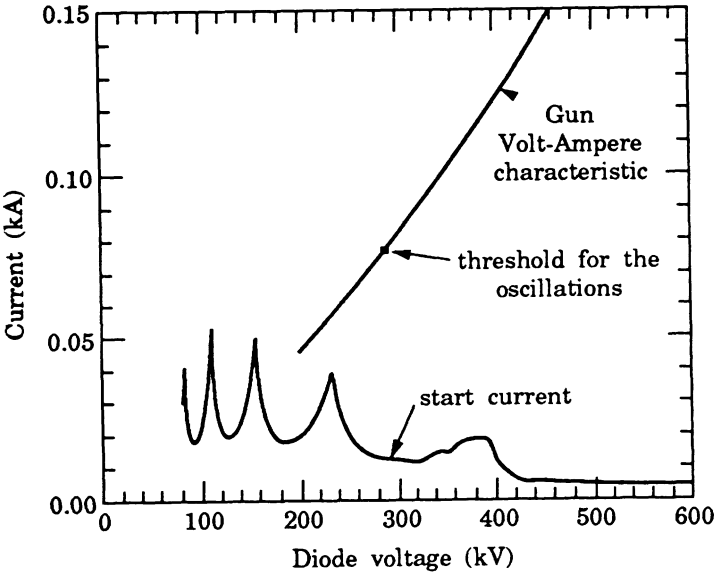

Fig. 3. The starting current in kA versus diode voltage in kV for the RF structure used in the experiment. The Gun Volt-Ampere characteristic with the black square marking the measured threshold conditions for the BWO.

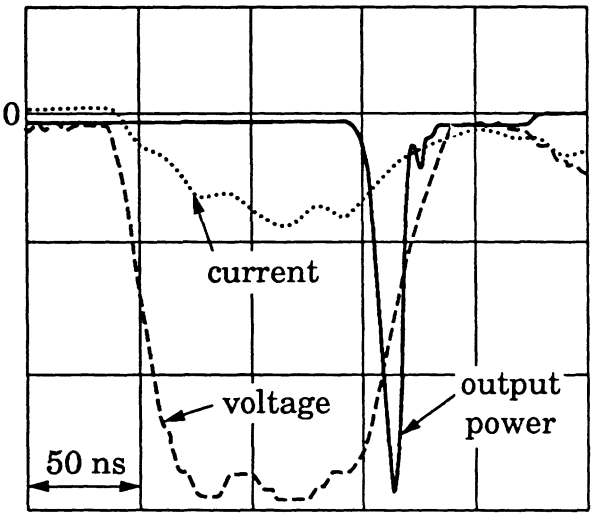

Fig. 4. The oscilloscope traces of the beam current versus time (dotted line) and the beam voltage (dashed line) and the radiated power (solid line).

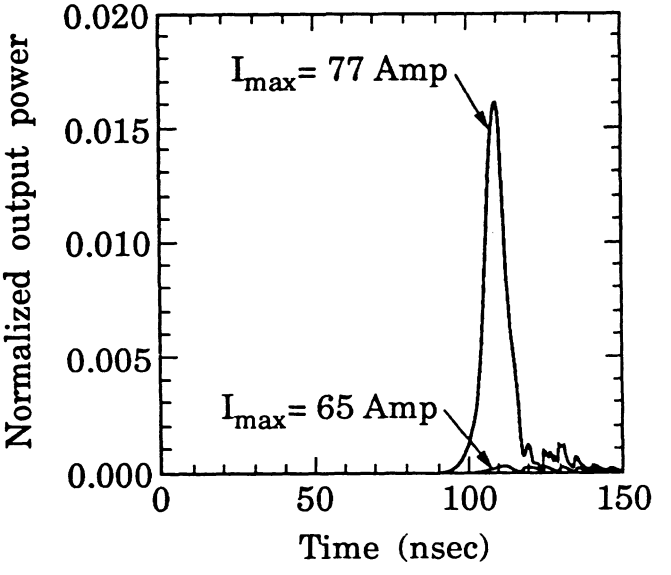

Fig. 5. The calculated normalized output power versus time in nsec for maximum current (a) 77 Amp and (b) 65 Amp.

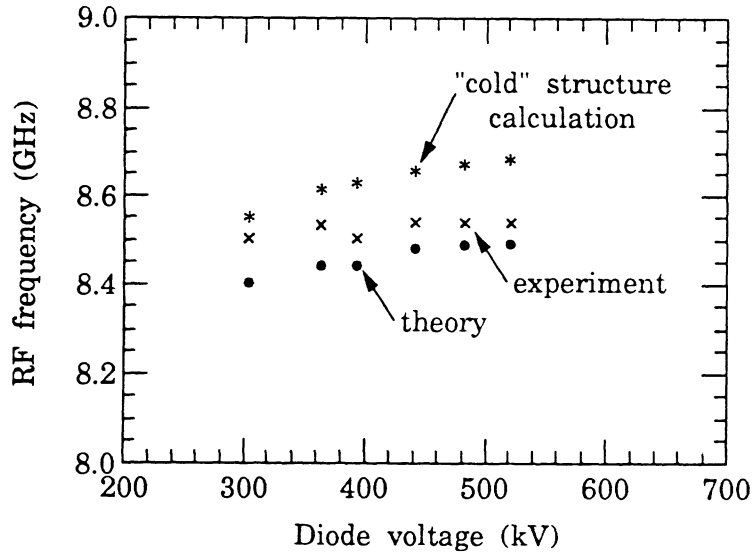

Fig. 6. Frequency of the BWO operation versus gun voltage (kV). The crosses are the measured frequency; the stars are the calculated frequency using cold structure dispersion curve; the solid dots are the calculated frequency using the nonlinear model.

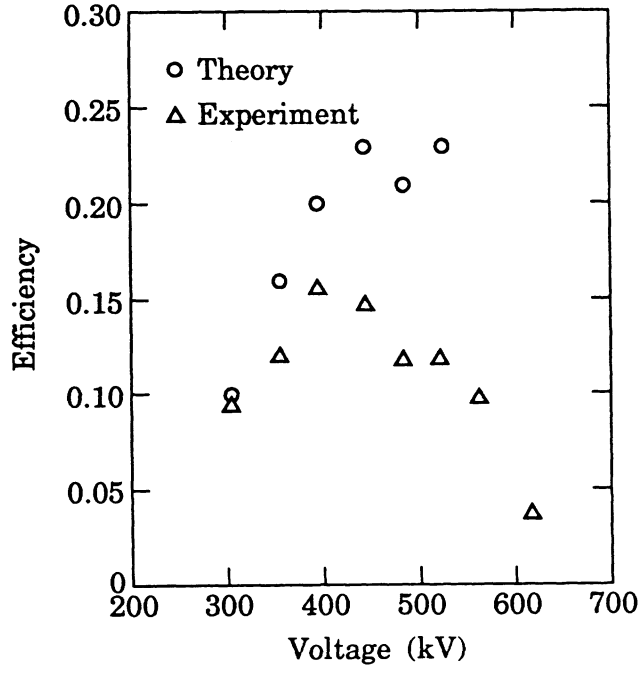

Fig. 7. The efficiency versus voltage (kV). The triangles are the ratio of the maximum measured RF power to the maximum beam power and the circles are the calculated peak efficiency.